Translational, rotational, vibrational and electron temperatures of a gliding arc discharge

Zhu, Jiajian; Ehn, Andreas; Gao, Jinlong; Kong, Chengdong; Aldén, Marcus; Salewski, Mirko; Leipold, Frank; Kusano, Yukihiro; Li, Zhongshan

Published in:
Optics Express

DOI:
10.1364/OE.25.020243

2017

Document Version:
Publisher's PDF, also known as Version of record

Research Article
Vol. 25, No. 17 | 21 Aug 2017 | OPTICS EXPRESS 20243
Optics EXPRESS

Translational, rotational, vibrational and electron temperatures of a gliding arc discharge

JIAJIAN ZHU,[1,2,*] ANDREAS EHN,[2] JINLONG GAO,[2] CHENGDONG KONG,[2] MARCUS ALDÉN,[2] MIRKO SALEWSKI,[3] FRANK LEIPOLD,[3] YUKIHIRO KUSANO,[4] AND ZHONGSHAN LI[2]

[1]*Science and Technology on Scramjet Laboratory, National University of Defense Technology, Changsha 410073, China*
[2]*Division of Combustion Physics, Lund University, P.O. Box 118, S-221 00 Lund, Sweden*
[3]*Department of Physics, Section for Plasma Physics and Fusion Energy, Technical University of Denmark DK-2800 Kgs. Lyngby, Denmark*
[4]*Department of Wind Energy, Section for Composites and Materials Mechanics, Technical University of Denmark, Risø Campus, Frederiksborgvej 399, DK-4000 Roskilde, Denmark*
[*]*jjzhu@nudt.edu.cn*

Abstract:Translational, rotational, vibrational and electron temperatures of a gliding arc discharge in atmospheric pressure air were experimentally investigated using in situ, non-intrusive optical diagnostic techniques. The gliding arc discharge was driven by a 35 kHz alternating current (AC) power source and operated in a glow-type regime. The two-dimensional distribution of the translational temperature (T_t) of the gliding arc discharge was determined using planar laser-induced Rayleigh scattering. The rotational and vibrational temperatures were obtained by simulating the experimental spectra. The OH A–X (0, 0) band was used to simulate the rotational temperature (T_r) of the gliding arc discharge whereas the NO A–X (1, 0) and (0, 1) bands were used to determine its vibrational temperature (T_v). The instantaneous reduced electric field strength *E/N* was obtained by simultaneously measuring the instantaneous length of the plasma column, the discharge voltage and the translational temperature, from which the electron temperature (T_e) of the gliding arc discharge was estimated. The uncertainties of the translational, rotational, vibrational and electron temperatures were analyzed. The relations of these four different temperatures ($T_e > T_v > T_r > T_t$) suggest a high-degree non-equilibrium state of the gliding arc discharge.

OCIS codes: (280.5395) Plasma diagnostics; (280.6780) Temperature; (350.5400) Plasmas; (290.5870) Scattering, Rayleigh; (300.2140) Emission; (300.6540) Spectroscopy, ultraviolet.

References and links

1. A. Fridman, S. Nester, L. A. Kennedy, A. Saveliev, and O. Mutaf-Yardimci, "Gliding arc gas discharge," Prog Energ Combust **25**(2), 211–231 (1999).
2. F. Richard, J. M. Cormier, S. Pellerin, and J. Chapelle, "Physical study of a gliding arc discharge," J. Appl. Phys. **79**(5), 2245–2250 (1996).
3. A. Czernichowski, "Gliding arc - applications to engineering and environment control," Pure Appl. Chem. **66**(6), 1301–1310 (1994).
4. J. Zhu, J. Gao, Z. Li, A. Ehn, M. Aldén, A. Larsson, and Y. Kusano, "Sustained diffusive alternating current gliding arc discharge in atmospheric pressure air," Appl. Phys. Lett. **105**(23), 234102 (2014).
5. T. Ombrello, X. Qin, Y. G. Ju, and C. Carter, "Combustion enhancement via stabilized piecewise nonequilibrium gliding arc plasma discharge," AIAA J. **44**(1), 142–150 (2006).
6. A. Fridman, A. Gutsol, S. Gangoli, Y. G. Ju, and T. Ombrellol, "Characteristics of Gliding Arc and Its Application in Combustion Enhancement," J. Propuls. Power **24**(6), 1216–1228 (2008).
7. D. H. Lee, K. T. Kim, M. S. Cha, and Y. H. Song, "Optimization scheme of a rotating gliding arc reactor for partial oxidation of methane," Proc. Combust. Inst. **31**(2), 3343–3351 (2007).
8. H. Zhang, C. Du, A. Wu, Z. Bo, J. Yan, and X. Li, "Rotating gliding arc assisted methane decomposition in nitrogen for hydrogen production," Int. J. Hydrogen Energy **39**(24), 12620–12635 (2014).

#296901 https://doi.org/10.1364/OE.25.020243
Journal © 2017 Received 29 May 2017; revised 29 Jul 2017; accepted 9 Aug 2017; published 11 Aug 2017

Optics EXPRESS

9. F. Zhu, H. Zhang, X. Yan, J. Yan, M. Ni, X. Li, and X. Tu, "Plasma-catalytic reforming of CO2-rich biogas over Ni/γ-Al2O3 catalysts in a rotating gliding arc reactor," Fuel **199**, 430–437 (2017).
10. X. Tu and J. C. Whitehead, "Plasma dry reforming of methane in an atmospheric pressure AC gliding arc discharge: Co-generation of syngas and carbon nanomaterials," Int. J. Hydrogen Energy **39**(18), 9658–9669 (2014).
11. A. Indarto, J. W. Choi, H. Lee, and H. K. Song, "Effect of additive gases on methane conversion using gliding arc discharge," Energy **31**(14), 2986–2995 (2006).
12. R. Burlica, R. G. Grim, K. Y. Shih, D. Balkwill, and B. R. Locke, "Bacteria Inactivation Using Low Power Pulsed Gliding Arc Discharges with Water Spray," Plasma Process. Polym. **7**(8), 640–649 (2010).
13. C. M. Du, J. Wang, L. Zhang, H. X. Li, H. Liu, and Y. Xiong, "The application of a non-thermal plasma generated by gas-liquid gliding arc discharge in sterilization," New J. Phys. **14**(1), 013010 (2012).
14. Y. Kusano, B. F. Sorensen, T. L. Andersen, H. L. Toftegaard, F. Leipold, M. Salewski, Z. W. Sun, J. J. Zhu, Z. S. Li, and M. Aldén, "Water-cooled non-thermal gliding arc for adhesion improvement of glass-fibre-reinforced polyester," J. Phys. D Appl. Phys. **46**(13), 135203 (2013).
15. Z. B. Feng, N. Saeki, T. Kuroki, M. Tahara, and M. Okubo, "Surface modification by nonthermal plasma induced by using magnetic-field-assisted gliding arc discharge," Appl. Phys. Lett. **101**(4), 041602 (2012).
16. Z. Bo, E. Wu, J. Yan, Y. Chi, and K. Cen, "Note: Gliding arc discharges with phase-chopped voltage supply for enhancement of energy efficiency in volatile organic compound decomposition," Rev. Sci. Instrum. **84**(1), 016105 (2013).
17. V. Dalaine, J. M. Cormier, S. Pellerin, and P. Lefaucheux, "H2S destruction in 50 Hz and 25 kHz gliding arc reactors," J. Appl. Phys. **84**(3), 1215–1221 (1998).
18. J. Gao, J. Zhu, A. Ehn, M. Aldén, and Z. Li, "In-Situ Non-intrusive Diagnostics of Toluene Removal by a Gliding Arc Discharge Using Planar Laser-Induced Fluorescence," Plasma Chem. Plasma Process. **37**(2), 433–450 (2017).
19. R. Burlica, M. J. Kirkpatrick, and B. R. Locke, "Formation of reactive species in gliding arc discharges with liquid water," J. Electrost. **64**(1), 35–43 (2006).
20. Y. G. Ju and W. T. Sun, "Plasma assisted combustion: Dynamics and chemistry," Prog Energ Combust **48**, 21–83 (2015).
21. Z. Yin, Z. Eckert, I. V. Adamovich, and W. R. Lempert, "Time-resolved radical species and temperature distributions in an Ar-O_2-H_2 mixture excited by a nanosecond pulse discharge," Proc. Combust. Inst. **35**(3), 3455–3462 (2015).
22. D. Staack, B. Farouk, A. F. Gutsol, and A. A. Fridman, "Spectroscopic studies and rotational and vibrational temperature measurements of atmospheric pressure normal glow plasma discharges in air," Plasma Sources Sci. Technol. **15**(4), 818–827 (2006).
23. I. V. Kuznetsova, N. Y. Kalashnikov, A. F. Gutsol, A. A. Fridman, and L. A. Kennedy, "Effect of "overshooting" in the transitional regimes of the low-current gliding arc discharge," J. Appl. Phys. **92**(8), 4231–4237 (2002).
24. O. Mutaf-Yardimci, A. V. Saveliev, A. A. Fridman, and L. A. Kennedy, "Thermal and nonthermal regimes of gliding arc discharge in air flow," J. Appl. Phys. **87**(4), 1632–1641 (2000).
25. A. Czernichowski, H. Nassar, A. Ranaivosoloarimanana, A. A. Fridman, M. Simek, K. Musiol, E. Pawelec, and L. Dittrichova, "Spectral and electrical diagnostics of gliding arc," Acta Phys. Pol. A **89**(5–6), 595–603 (1996).
26. B. Benstaali, P. Boubert, B. G. Cheron, A. Addou, and J. L. Brisset, "Density and rotational temperature measurements of the OH degrees and NO degrees radicals produced by a gliding arc in humid air," Plasma Chem. Plasma Process. **22**(4), 553–571 (2002).
27. T. L. Zhao, Y. Xu, Y. H. Song, X. S. Li, J. L. Liu, J. B. Liu, and A. M. Zhu, "Determination of vibrational and rotational temperatures in a gliding arc discharge by using overlapped molecular emission spectra," J. Phys. D Appl. Phys. **46**(34), 345201 (2013).
28. S. P. Gangoli, A. F. Gutsol, and A. A. Fridman, "A non-equilibrium plasma source: magnetically stabilized gliding arc discharge: I. Design and diagnostics," Plasma Sources Sci. Technol. **19**(6), 065003 (2010).
29. C. O. Laux, T. G. Spence, C. H. Kruger, and R. N. Zare, "Optical diagnostics of atmospheric pressure air plasmas," Plasma Sources Sci. Technol. **12**(2), 125–138 (2003).
30. C. Zhang, T. Shao, P. Yan, and Y. X. Zhou, "Nanosecond-pulse gliding discharges between point-to-point electrodes in open air," Plasma Sources Sci. Technol. **23**(3), 035004 (2014).
31. Y. D. Korolev, O. B. Frants, N. V. Landl, A. V. Bolotov, and V. O. Nekhoroshev, "Features of a near-cathode region in a gliding arc discharge in air flow," Plasma Sources Sci. Technol. **23**(5), 054016 (2014).
32. S. P. Gangoli, A. F. Gutsol, and A. A. Fridman, "A non-equilibrium plasma source: magnetically stabilized gliding arc discharge: II. Electrical characterization," Plasma Sources Sci. Technol. **19**(6), 065004 (2010).
33. Y. D. Korolev, O. B. Frants, V. G. Geyman, N. V. Landl, and V. S. Kasyanov, "Low-Current "Gliding Arc" in an Air Flow," IEEE Trans. Plasma Sci. **39**(12), 3319–3325 (2011).
34. J. Šperka, P. Souček, J. J. W. A. Van Loon, A. Dowson, C. Schwarz, J. Krause, G. Kroesen, and V. Kudrle, "Hypergravity effects on glide arc plasma," Eur. Phys. J. D **67**(12), 261 (2013).
35. L. Potočňáková, J. Šperka, P. Zikán, J. J. W. A. van Loon, J. Beckers, and V. Kudrle, "Gravity effects on a gliding arc in four noble gases: from normal to hypergravity," Plasma Sources Sci. Technol. **24**(2), 022002 (2015).

Optics EXPRESS

36. N. C. Roy, M. G. Hafez, and M. R. Talukder, "Characterization of atmospheric pressure H_2O/O_2 gliding arc plasma for the production of OH and O radicals," Phys. Plasmas **23**(8), 083502 (2016).
37. J. Zhu, Z. Sun, Z. Li, A. Ehn, M. Alden, M. Salewski, F. Leipold, and Y. Kusano, "Dynamics, OH distributions and UV emission of a gliding arc at various flow-rates investigated by optical measurements," J. Phys. D Appl. Phys. **47**(29), 295203 (2014).
38. Z. W. Sun, J. J. Zhu, Z. S. Li, M. Aldén, F. Leipold, M. Salewski, and Y. Kusano, "Optical diagnostics of a gliding arc," Opt. Express **21**(5), 6028–6044 (2013).
39. S. Kolev, S. Sun, G. Trenchev, W. Wang, H. Wang, and A. Bogaerts, "Quasi-Neutral Modeling of Gliding Arc Plasmas," Plasma Process. Polym. **14**(4–5), 1600110 (2017).
40. S. R. Sun, S. Kolev, H. X. Wang, and A. Bogaerts, "Investigations of discharge and post-discharge in a gliding arc: a 3D computational study," Plasma Sources Sci. Technol. **26**(5), 055017 (2017).
41. S. Pellerin, F. Richard, J. Chapelle, J. M. Cormier, and K. Musiol, "Heat string model of bi-dimensional dc Glidarc," J. Phys. D Appl. Phys. **33**(19), 2407–2419 (2000).
42. P. J. Bruggeman, N. Sadeghi, D. C. Schram, and V. Linss, "Gas temperature determination from rotational lines in non-equilibrium plasmas: a review," Plasma Sources Sci. Technol. **23**(2), 023001 (2014).
43. A. Ehn, J. Zhu, X. Li, and J. Kiefer, "Advanced Laser-Based Techniques for Gas-Phase Diagnostics in Combustion and Aerospace Engineering," Appl. Spectrosc. **71**(3), 341–366 (2017).
44. J. Zhu, J. Gao, A. Ehn, M. Aldén, A. Larsson, Y. Kusano, and Z. Li, "Spatiotemporally resolved characteristics of a gliding arc discharge in a turbulent air flow at atmospheric pressure," Phys. Plasmas **24**(1), 013514 (2017).
45. J. Zhu, J. Gao, A. Ehn, M. Aldén, Z. Li, D. Moseev, Y. Kusano, M. Salewski, A. Alpers, P. Gritzmann, and M. Schwenk, "Measurements of 3D slip velocities and plasma column lengths of a gliding arc discharge," Appl. Phys. Lett. **106**(4), 044101 (2015).
46. S. Pellerin, J. M. Cormier, F. Richard, K. Musiol, and J. Chapelle, "A spectroscopic diagnostic method using UV OH band spectrum," J. Phys. D Appl. Phys. **29**(3), 726–739 (1996).
47. G. J. M. Hagelaar and L. C. Pitchford, "Solving the Boltzmann equation to obtain electron transport coefficients and rate coefficients for fluid models," Plasma Sources Sci. Technol. **14**(4), 722–733 (2005).
48. A. V. Phelps and L. C. Pitchford, "Anisotropic scattering of electrons by N2 and its effect on electron transport," Phys. Rev. A Gen. Phys. **31**(5), 2932–2949 (1985).
49. SIGLO database, http://www.lxcat.laplace.univ-tlse.fr, retrieved June 4, 2013.
50. A. P. Yalin, Y. Z. Ionikh, and R. B. Miles, "Gas temperature measurements in weakly ionized glow discharges with filtered Rayleigh scattering," Appl. Opt. **41**(18), 3753–3762 (2002).
51. X. Tu, L. Yu, J. H. Yan, K. F. Cen, and B. G. Cheron, "Dynamic and spectroscopic characteristics of atmospheric gliding arc in gas-liquid two-phase flow," Phys. Plasmas **16**(11), 113506 (2009).
52. E. Kristensson, A. Ehn, J. Bood, and M. Alden, "Advancements in Rayleigh scattering thermometry by means of structured illumination," Proc. Combust. Inst. **35**(3), 3689–3696 (2015).

1. Introduction

Gliding arc discharges provide a simple and low-cost method for generating atmospheric pressure plasma discharges [1–4]. During the past decades gliding arc discharges have been widely used in combustion enhancement [5–7], gas conversion and decomposition [8–11], bacterial inactivation [12, 13], surface treatment [14, 15] and pollution control [16–18]. Many of these applications rely on the formation of reactive species that can increase chemical reaction rates [19, 20]. Reactive species, such as free radicals, excited species and free electrons, can be effectively produced in non-thermal plasmas [21], which are characterized by different translational, rotational, vibrational and electron temperatures. Excessive gas heating is significantly suppressed in non-thermal plasmas, so that energy is mostly used for producing reactive species [22].

It was reported that gliding arc discharges can be used to create non-thermal plasmas [23, 24], and the non-thermal properties of gliding arc discharges can be quantified by different translational, rotational, vibrational and electron temperatures. Czernichowski and associates [25] obtained the vibrational temperature (~3000 K) and the rotational temperature (1000 – 1500 K) of a non-thermal gliding arc discharge by comparing the measured and fitted emission spectra of the N_2 (C–B, $\Delta\upsilon = -2, -1, 0$) bands. In addition, its electron temperature (~10000 K) was estimated from the measured reduced electric field strength whereas the translational temperature was assumed to be close to the rotational temperature in their work. Benstaali et al. [26] used the NO A–X (0, 1) and OH A–X (0, 0) bands to determine the rotational temperature (2400 – 3600 K) of a gliding arc discharge in humid air. It was found that the rotational temperature decreased linearly as the distance of the narrowest gap of the electrodes increased. Transition bands from different species may overlap as the translational

Optics EXPRESS

temperature increases, such as the N_2 (C–B, $\Delta v = 1$) overlap with the OH (A–X, $\Delta v = 1$) in the range of 305-320 nm, and the N_2 (C–B, $\Delta v = -2, -3$) overlap with the N_2^+ (B–X, $\Delta v = 0$) in the range 370-395 nm. Zhao and associates [27] extracted individual spectra from these overlapping bands so as to simulate the vibrational and rotational temperatures of a kHz alternating current (AC) gliding arc discharge. It was found that the rotational and vibrational temperatures were dependent on the species that were used in analysis. Fridman et al. [6,28] calculated the rotational (~2200-2500 K) and vibrational (~3200-3700 K) temperatures of a magnetically stabilized gliding arc discharge by simulating the experimental OH (A–X) and N_2 (C–B) bands using the SPECAIR program [29].

Substantial progress in studying gliding arc discharges has been achieved, including transient discharge processes [30, 31], electrical characteristics [32, 33], hypergravity effects [34, 35] and species distributions [36–38], as well as the rotational and vibrational temperatures of gliding arc discharges [25–28]. However, the translational temperature of the gliding arc discharge has not been directly measured yet up to now. The translational temperature of the gliding arc discharge is usually obtained from modeling [39–41] or estimated to be equal to the rotational temperature based on the assumption of a fast rotational-translational relaxation [25]. However, as Bruggeman and associates pointed out [42], the rotational-translational equilibrium is not always valid in non-thermal plasmas, and determination of the translational temperature from emission spectra should be made with a caution. The translational temperature can be directly measured using laser-induced Rayleigh scattering technique [43]. This technique is regarded as a useful tool for determination of the translational temperature of non-thermal atmospheric pressure plasmas with good accuracy [42].

The translational temperature is required to be compared with rotational, vibrational and electron temperatures in order to clearly characterize non-thermal properties of the gliding arc discharge. The rotational and vibrational temperatures can be deduced from emission spectra of the gliding arc discharge. In addition, the electron temperature can be calculated using the reduced electric field strength that is dependent on simultaneous measurements of both the electric field strength and the translational temperature. In our earlier work, an AC gliding arc discharge was generated in atmospheric air, and temporally [37, 44], spatially [45] and spectrally [38] resolved characteristics of the gliding arc discharge in atmospheric air were experimentally investigated. Glow-type and spark-type discharges can be recognized during the evolution of the gliding arc discharge [37, 44]. The glow-type discharges are characterized by current peaks of hundreds of milliamperes whereas the spark-type discharges are recognized by current spikes of up to tens of amperes [44]. The glow-type discharges were found to be effective in surface treatment [14] and toluene removal [18]. However, non-thermal properties of the glow-type gliding arc discharge are still unclear mainly due to the lack of information about its translational, rotational, vibrational and electron temperatures.

In this study, translational, rotational, vibrational and electron temperatures of glow-type gliding arc discharges in atmospheric air were experimentally investigated. First, planar laser-induced Rayleigh scattering was conducted to obtain the translational temperature of the gliding arc discharge. Second, the rotational and vibrational temperatures were obtained by simulating the experimentally measured emission spectra from the OH A–X (0, 0) band and the NO A–X (1, 0) and (0, 1) bands. Third, the translational temperature, the length of the plasma column, and the voltage over the gliding arc discharge were measured simultaneously so as to determine the reduced electric field strength and to estimate the electron temperature.

Optics EXPRESS

2. Methods

The translational temperature of the gliding arc discharge was measured by planar laser-induced Rayleigh scattering. The intensity of the Rayleigh scattering signal I_R from a gas mixture can be expressed as

$$I_R = CI_0 N\sigma \tag{1}$$

where C is a constant determined by the collection efficiency and the probe volume of the experimental setup, I_0 the incident laser intensity, N the number density and σ the Rayleigh cross section of the mixture. Substituting the ideal gas law $N = P/kT$ into Eq. (1) gives

$$I_R = \frac{CI_0 P\sigma}{kT} \tag{2}$$

where P is the pressure, T is the translational temperature and k is the Boltzmann constant. For determining the translational temperature of a gliding arc discharge, the Rayleigh signal scattered from air at the room temperature (298 K) is used to normalize the constant C and the incident laser intensity I_0. The Rayleigh cross section of the mixture is determined by the major constitutes and their relative abundance. It should be noted that species like OH, NO, N_2* and O_3 can be generated by the gliding arc discharge in air. However, since the gliding arc discharge is weakly ionized [4, 32], the influence of these minor species on the Rayleigh cross section can be neglected. It is thus reasonable to consider only the major species (O_2 and N_2 in air) for calculating the Rayleigh cross section. The translational temperature of the gliding arc discharge can be written as

$$T_t = \frac{I_a - I_b}{I_g - I_b} T_0 \tag{3}$$

where I_a, I_g, I_b, and T_0 represent the Rayleigh signal from the air, the Rayleigh signal from the gliding arc discharge, the background signal measured with the laser switched off and the air temperature (298 K), respectively. It is noted that the measurements of I_a and I_b were conducted with the gas flow on and with the gliding arc discharge off.

The rotational and vibrational temperature can be obtained by simulating the experimental emission spectra. The simulated spectra are obtained by use of the SPECAIR (version 3.0) [29], which models emission spectra of species that are generated in air plasmas, such as N_2, O_2, NO, N_2^+, N, NH, O and OH. Predominant spectral features of NO (A–X) and OH (A–X) were experimentally observed in the emission spectra of the gliding arc discharge in air at a low flow rate in our previous work [37, 38], and so they are chosen to determine the rotational and vibrational temperatures. A slit function, as an important input parameter to the SPECAIR, is used to evaluate the instrumental broadening that significantly affects the temperature determination [46]. The slit function (FWHM = 0.25 nm) used in this work was experimentally obtained by using a HeNe laser at 632.8 nm.

The electron temperature can be calculated using BOLSIG + [47]. The BOLSIG + is a solver of the Boltzmann equation, which can be used to calculate electron coefficients of weakly ionized gas discharges. The calculation mainly relies on various collision cross sections of the molecules. In this work, the newest version of the BOLSIG + (Version 03/2016) was used to calculate the electron temperature of the gliding arc discharge and the data sets of the collision cross section were taken from LXCat [48, 49]. In addition, the calculation of the electron temperature by means of BOLSIG + depends on the reduced electric field strength E/N, which can be expressed as

$$\frac{E}{N} = \frac{kVT_t}{LP} \tag{4}$$

Optics EXPRESS

where V is the voltage drop of the plasma column, L is the length of the plasma column, P is the atmospheric pressure (1.01×10^5 Pa), k is the Boltzmann constant (1.38×10^{-23} $J\ K^{-1}$) and T_t is the translational temperature. It should be noted that the voltage V, the length L, and the translational temperature T_t need to be measured simultaneously so as to obtain an accurate reduced electric field strength.

3. Experimental setup

A schematic of the experimental arrangement is shown in Fig. 1(a), in which measurements of the translational temperature and the length of the plasma column, as well as the current and the voltage can be conducted simultaneously. The gliding arc discharge in atmospheric air was driven by a 35 kHz AC power supply (Generator 9030E, SOFTAL Electronic GmbH, Germany) with a rated input power of 800 W, and it was generated between two diverging electrodes with a minimum distance of 7 mm. The electrodes are made of stainless steel tubes with an outer diameter of 3 mm that were cooled internally by water. A similar gliding arc discharge system has been described in our previous work [4, 37, 44, 45]. An air flow was fed through a 3 mm-diameter circular nozzle between the two electrodes to extend the plasma column in an upward direction. The air flow rate was controlled at 17.5 standard liter per minute (SLM) by a mass flow controller. At this input power and flow rate, the glow-type discharge dominates whereas the spark-type discharges can be just identified occasionally [37, 44]. In this work, temperatures of the glow-type discharge are measured due to the fact that the glow-type discharges can be dominantly observed at 17.5 SLM and 800 W. In addition, the glow-type discharges are more likely to be captured by a low-frequency laser (10 Hz) used in the Rayleigh measurements.

A 10 Hz frequency-doubled Nd:YAG laser (Quantel, Brilliant b) at 532 nm with an output energy of about 350 mJ/pulse was used to perform the Rayleigh scattering measurements. The laser beam was transmitted through a cylindrical lens (CL, f = –40 mm) and a spherical lens (SL, f = 200 mm) to form a laser sheet with a thickness of about 0.1 mm and a height of 30 mm, which enables the laser sheet to be located at 67-97 mm above the exit of the 3 mm-diameter circular nozzle. The laser sheet was directed through the gliding arc discharge to generate the Rayleigh scattering signal. The Rayleigh scattering signal was collected by an ICCD camera (ICCD1 in Fig. 1(a), Princeton PI-MAX II) equipped with an objective lens (Nikkon f = 105 mm). The exposure time of the ICCD camera for collecting both the Rayleigh scattering signal and the plasma column emission signal is set to 2 μs, whereas that for recording the pure Rayleigh scattering signal was set to 30 ns so as to significantly suppress spontaneous emission from the gliding arc discharge.

Another ICCD camera (ICCD2 in Fig. 1(a), Princeton PI-MAX II) mounted with an objective lens (UV Nikkon f = 105 mm) was operated at a 3 μs exposure time to record images of plasma columns. The delay of the camera gate was adjusted to not capture the laser beam. A current monitor (Pearson Electronics, model 6585) and a voltage probe (Tektronix P6015A) were used for measuring the current and the voltage. Both the current and the voltage signal were simultaneously recorded by use of a four-channel oscilloscope (PS, PicoScope 4424).

The Rayleigh signal, the image of the plasma column, as well as the current and the voltage waveforms were obtained simultaneously by the precisely timed external triggering. A pulse generator (1st PG, BNC 575) generates a seed trigger pulse, externally triggering the power supply and another pulse generator (2nd PG, DG 535). Two channels of the second pulse generator externally trigger the flash lamp and the Q-switch of the Nd:YAG laser, respectively. The Q-switch of the laser is used to trigger the two ICCD cameras. The gate monitor signal of the second ICCD camera is employed to trigger the third pulse generator (BNC 555) that is used to trigger the PicoScope (PS). The timing for experimental measurements is illustrated in Fig. 1(b). The experimental measurements were carried out about 10 ms after the gliding arc was ignited, which ensures that the gliding arc can be

Optics EXPRESS

extended to the probe volume by the air flow. A fine adjustment of the delay time was conducted by the ICCD cameras to precisely capture the same peak of the sinusoidal AC driving signal in every set of measurements.

Emission spectra of the gliding arc discharge are captured to simulate the rotational and vibrational temperatures. Figure 1(c) displays a schematic of the experimental arrangement for spectrometric measurements. The emission was collected and focused into the slit of a spectrometer with a spectral resolution of 0.18 nm (Shamrock 750i, Andor, 300 grooves/mm grating) mounted with an ICCD camera (iStar, Andor) by use of two spherical lenses (f = 150 mm and f = 200 mm). The ICCD camera for the spectroscopic measurements was set to an exposure time of 100 μs and was synchronized to the driving signal of the gliding arc discharge. The delay time between the ICCD camera and the driving signal of the gliding arc discharge was adjusted by a pulse generator (DG535). An appropriate delay time (10 ms) was used to more frequently capture the emission of the plasma column. 200 data acquirisitions for each case were accumulated by the ICCD-based imaging spectrometer. The slit of the spectrometer was vertically oriented, allowing the ICCD camera to observe a spatially resolved height range of 4 cm (7-11 cm above the exit of the 3 mm-diameter circular nozzle). The spectral response of the spectrometer was calibrated by means of a mercury lamp.

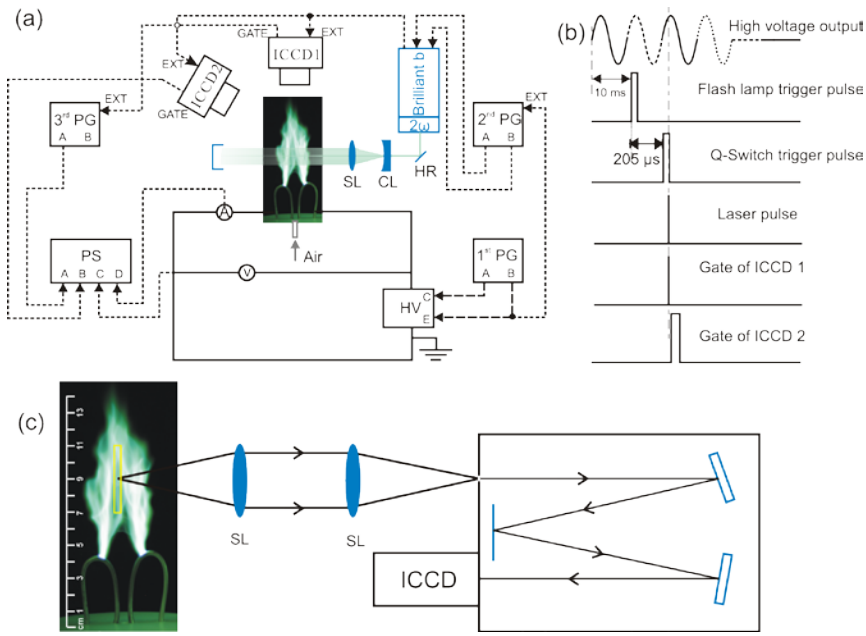

Fig. 1. (a) Experimental setup for simultaneous measurements of translational temperature, the current, the voltage, and the length of the plasma column. HV: high voltage power supply; PS: 4-channel PicoScope; PG: pulse generator; (b) Timing for measurements shown in (a); (c) Experimental setup for spectrometric measurements.

4. Results and discussion

The translational, rotational, vibrational and electron temperatures of the gliding arc discharge in atmospheric air were obtained using planar laser-induced Rayleigh scattering, emission spectra and BOLSIG + simulation, respectively.

4.1 Translational temperature

Both the plasma emission and the Rayleigh scattering signals can be simultaneously recorded using an ICCD camera with a 2 μs acquisition time. Figures 2(a_1) – 2(c_1) display three single-

Optics EXPRESS

shot images in which both the plasma emission and the Rayleigh scattering signals can be seen. The emission of the plasma column takes the form of string-like channels, and the plasma emission in the string-like channels dominates. In the vicinity of the plasma column, the pure Rayleigh scattering signal was collected. The Rayleigh scattering signals are distributed unevenly around the plasma channel. The intensity of the Rayleigh scattering signal around the plasma channel is relatively weak, indicating that the hot gases are located at this region. The intensity of the Rayleigh signal is dependent on the Rayleigh cross section which is determined by the gas composition in the probe volume. The major scattering species is air with or without the gliding arc plasma present since the electron density of the plasma is rather low. Further, it should be emphasized that the laser sheet with a two-dimensional structure is fixed at the focal plane of the ICCD camera whereas the plasma column of the gliding arc discharge with a transient three-dimensional character moves into the field of view of the ICCD camera. Thus, adequate translational temperature images can be acquired when the gliding arc crosses the laser sheet, as shown in Figs. $2(a_1) – 2(c_1)$.

The Rayleigh scattering signal can be used to calculate the translational temperature according to Eq. (3). Figures $2(a_2) – 2(c_2)$ shows two-dimensional temperature distributions in the vicinity of the plasma column, which are calculated by use of the Rayleigh scattering signals shown in Figs. $2(a_1) – 2(c_1)$, respectively. The colorbar here represents the values of the translational temperature in the vicinity of the plasma column. It should be noted that the temperature in the plasma channel is inaccurate due to the strong plasma emission that interferes with the Rayleigh scattering. The hot region is distributed in the vicinity of the plasma column. The typical size of the hot region (> 500 K) is labeled in these figures. The size of the hot region is estimated to be about 4 – 11 times greater than the width of the plasma column (less than 1 mm). The plasma column is heated by the current, and the generated heat is transported from the hot plasma column to its neighboring region due to turbulent convection. In other words, the plasma column can heat the surrounding gas and so the Rayleigh scattering probes a much wider hot region area than the exact plasma column detected by the plasma emission.

The strong plasma emission can interfere with an accurate determination of the translational temperature. Fortunately, the plasma emission can be rejected effectively by use of the ICCD camera with an acquisition time of 30 ns. It is a conventional method to use an ICCD camera with an extremely short exposure time to capture exactly pulsed signals (i.e., the Rayleigh scattering signals) and to suppress a continuous background (i.e., the plasma emissions). The two-dimensional distribution of the translational temperature of a typical gliding arc discharge is shown in Fig. 3(a) together with the plasma column and the electrical parameters. Figure $3(a_1)$ shows the translational temperature distribution of a typical gliding arc discharge. The plasma channel is invisible here due to significant suppression of the plasma emission by the 30 ns acquisition time. Lines of constant temperature are labeled in the hot region of the plasma. The temperature contour lines separate the hot regions with different temperatures, and the number on each contour line shows the temperature, such as 500, 700 and 900 K. Figure $3(a_2)$ shows the axial (the height axis) temperature profile whereas Fig. $3(a_3)$ shows the radial temperature profile. The temperature peaks at about 1500 K and then it decreases to about 500 K at a distance of 9 mm in the axial direction and of 11 mm in the radial direction. The image of the plasma column is simultaneously recorded by a second ICCD camera, as shown in Fig. $3(a_4)$. The field of view for recording the Rayleigh scattering signal is marked by a rectangle in this figure. The current and the voltage of the gliding arc discharge are also measured simultaneously. Figure $3(a_5)$ shows that the current of the plasma column is about 0.2 A and its voltage is approximately 4950 V, suggesting that the gliding arc discharge is operated in a glow mode.

Figure 3(b) exhibits a second example of the experimental results regarding the distribution of the translational temperature, the image of the plasma column, as well as the electrical parameters. As shown in Fig. $3(b_1)$, the predominantly hot regions are distributed in

Optics EXPRESS

two separated areas, corresponding to two parts of the plasma column shown in Fig. 3(b_4). The axial temperature profile and the radial temperature profile are displayed in Figs. 3(b_2) and 3(b_3), respectively, the largest temperature being about 1200 K. Figure 3(b_5) shows that the current and the voltage for the plasma column are about 0.18 A and 6850 V, respectively. It should be noted that there exits a significant voltage drop across the sheath region of the glow-type discharge. The voltage drop of a low-current gliding arc discharge operated at a glow-type regime was reported to be about 300 V [31, 33]. In this work, a voltage drop of 300 V is taken into consideration when calculating the reduced electric field strength using Eq. (4).

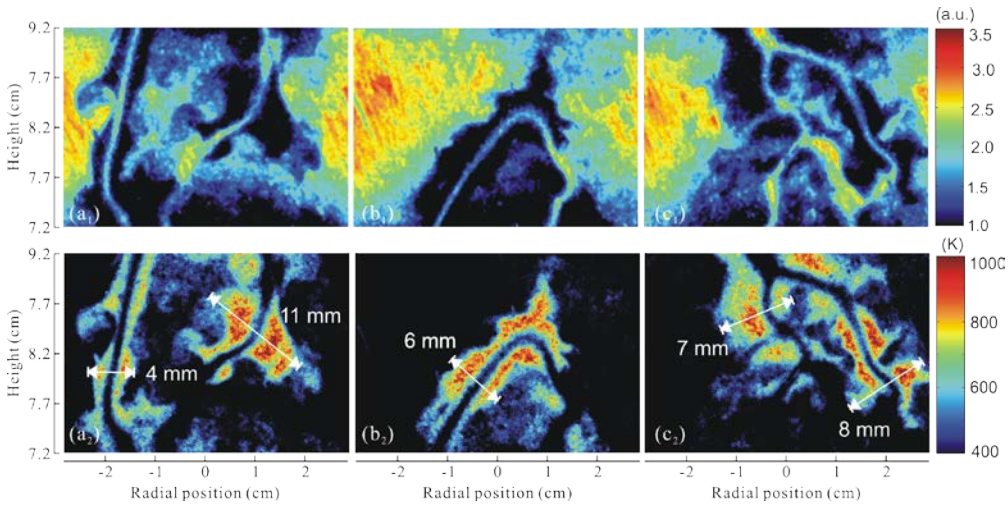

Fig. 2. (a_1) – (c_1): Two-dimensional distribution of the Rayleigh scattering signal and the plasma emission; (a_2) – (c_2): Two-dimensional distribution of the translational temperatures that are calculated by use of the Rayleigh scattering signal shown in Figs. 2(a_1) – 2(c_1), respectively. The colorbar in Figs. 2(a_1) – 2(c_1) shows the intensity (arb. units) of the plasma emission signal (in the plasma column) and the Rayleigh scattering signal (in the vicinity of the plasma column) whereas that in Figs. 2(a_2) – 2(c_2) indicates the translational temperature (K) in the vicinity of the plasma column. For this specific experimental setting (an acquisition time of 2 μs), the translational temperature in the plasma column cannot be accurately shown due to interference from strong plasam emission. Typical sizes of the hot regions around the plasma columns are labeled. The acquisition time of the ICCD camera is set to 2 μs in order to collect both the Rayleigh scattering signal and the plasma emission signal.

The translational temperature obtained from the Rayleigh scattering measurements are compared with other Rayleigh measurements. Yalin and associates [50] conducted translational temperature measurements in a low-pressure (~50 Torr) and weakly ionized glow discharge by using Rayleigh scattering techniques. In their work, a maximum translational temperature of about 800 K was recognized for the low-pressure glow discharge with a current of 30 mA. In our case, the maximum temperature measured by Rayleigh scattering is about 1500 K. This difference seems reasonable since our glow-type discharge has a larger current of 200 mA.

4.2 Rotational and vibrational temperatures

The rotational and vibrational temperatures of the gliding arc discharge can be obtained by stimulating the experimental emission spectra. The emission spectra of the OH A–X (0, 0) band are proper for simulating the rotational temperature [29, 46]. The simulated OH A–X (0, 0) bands at different rotational temperatures by means of SPECAIR are shown in the Fig. 4(a). The emission intensity is normalized by the peak at about 309 nm. It can be seen that the OH (A–X) (0, 0) band is sensitive to the rotational temperature and that the R branch and

Optics EXPRESS

the P branch are peaked at about 307 and 309 nm, and the ratio (P/R) of the peak intensities of the P and R branches have strong dependence on the rotational temperature, as shown in Fig. 4. The ratio of the P/R branch peak intensity of the experimental OH spectrum is marked by a square. The experimental ratio corresponds to a rotational temperature of about 4300 K. The simulated spectra at 4300 K rotational temperature were obtained by employing the SPECAIR. Both the experimental and modeled spectra of the OH (A–X) (0, 0) band are displayed in Fig. 4(b). It is found that a simulated spectrum for a rotational temperature of 4300 K agrees well with the experimental spectrum.

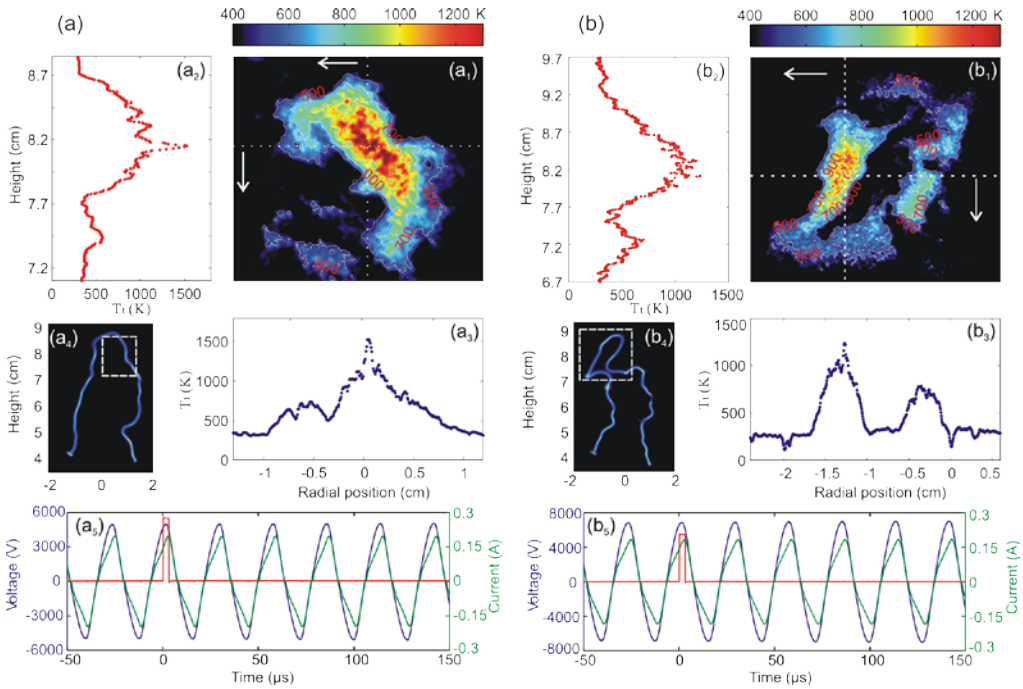

Fig. 3. Two examples of experimental results of a gliding arc discharge regarding the distribution of the translational temperature, the image of the plasma column, as well as waveforms of the current and voltage. (a_1), (b_1): Two-dimensional distribution of the translational temperature imaging; (a_2), (b_2): Axial temperature profile; (a_3), (b_3): Radial temperature profile; (a_4), (b_4): Image of the plasma column; (a_5), (b_5): the waveform of the voltage and the current. The temperature contour lines are shown in Figs. 3(a_1) and 3(b_1), and the number on each contour line shows the temperature (500, 700 and 900 K). A rectangle marked in Figs. 3(a_4) and 3(b_4) indicates the field of view for recording the Rayleigh scattering signal. The acquisition time of the ICCD camera for recording the pure Rayleigh scattering signal is 30 ns in order to significantly suppress the emission of the plasma column. The acquisition time for obtaining the image of the plasma column is 3 μs. A positive square marked in Figs. 3(a_5) and 3(b_5) represents the 3 μs acquisition time for recording the image of the plasma column. The simultaneous multi-parameter measurements (SMM) of the translational temperature, the voltage and the length of the plasma column allows for accurate determinations of the reduced electric field strength.

The experimental results show that the rotational temperature measured by optical emission spectroscopy (OES) is up to 3000 K larger than the translational temperature measured by Rayleigh scattering techniques. The large difference between the translational temperature and the rotational temperature indicates that the rotational-translational equilibrium is not established in our gliding arc discharge. Tu and associates [51] also found that their gliding arc discharge is not in the rotational-translational equilibrium as the rotational temperature of the gliding arc discharge was about 3000 K higher than its translational temperature. Whether the rotational-translational equilibrium exists, depends on

Optics EXPRESS

the relations between the effective lifetime of the excited state of interest and the rotational relaxation time [42, 51]. If the effective lifetime of the excited state is much smaller than the rotational relaxation time, the gliding arc discharge is not in the rotational-translational equilibrium. It should be noted that the Rayleigh scattering technique measured the spatially-resolved translational temperature distributions when the gliding arc discharge crosses the laser sheet in the focal plane of the ICCD camera. The emission spectroscopy technique acquired the line-of-sight rotational temperature of the gliding arc discharge. The thickness of the plasma column of the gliding arc discharge is quite small (less than 1 mm) and so the line-of-sight effects are not significant.

The NO A–X transition at a wavelength range of 211 – 239 nm is chosen to determine the vibrational temperature of the gliding arc discharge. The simulated and normalized NO emission spectra at different vibrational temperatures are shown in the Fig. 5(a). Three distinct peaks are observed in the NO emission spectra. The relative intensity of the NO A – X (1, 0) band at about 214.7 nm and the NO A–X (0, 1) band at about 236 nm is found to be sensitive to the vibrational temperature. Figure 5 exhibits the dependence of the vibrational temperature on the ratio of the two peak intensities of the (1, 0) and (0, 1) bands. The ratio of the two peak intensities of the experimental spectrum is shown as a square, indicating a vibrational temperature of approximately 5900 K. The experimental NO spectrum is shown in the Fig. 5(b) together with a corresponding simulated NO spectrum. The simulated spectrum was obtained at a vibrational temperature of 5900 K.

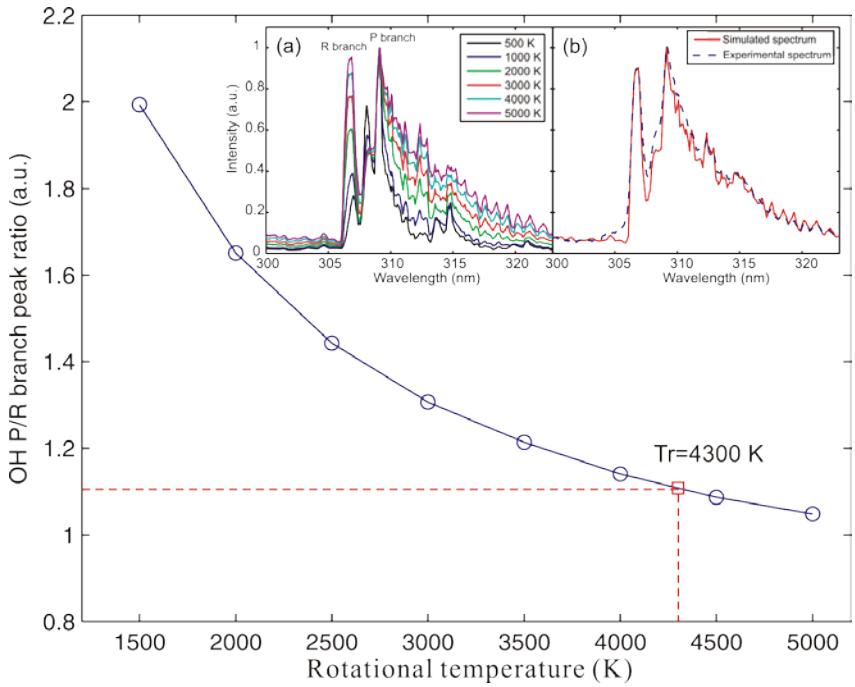

Fig. 4. Dependence of the rotational temperature on the peak ratio of the P and R branches of OH A–X (0, 0) bands. The circles show the simulated ratios at different rotational temperatures. The square represents the P/R branch peak ratio of the experimental OH A–X (0, 0) band, yielding an estimate of the rotational temperature of 4300 K. Figure 4(a) shows the simulated OH A–X (0, 0) bands at different rotational temperatures. Figure 4(b) shows the experimental OH spectrum of the gliding arc discharge and the simulated spectrum that was modeled at 4300 K rotational temperature.

Optics EXPRESS

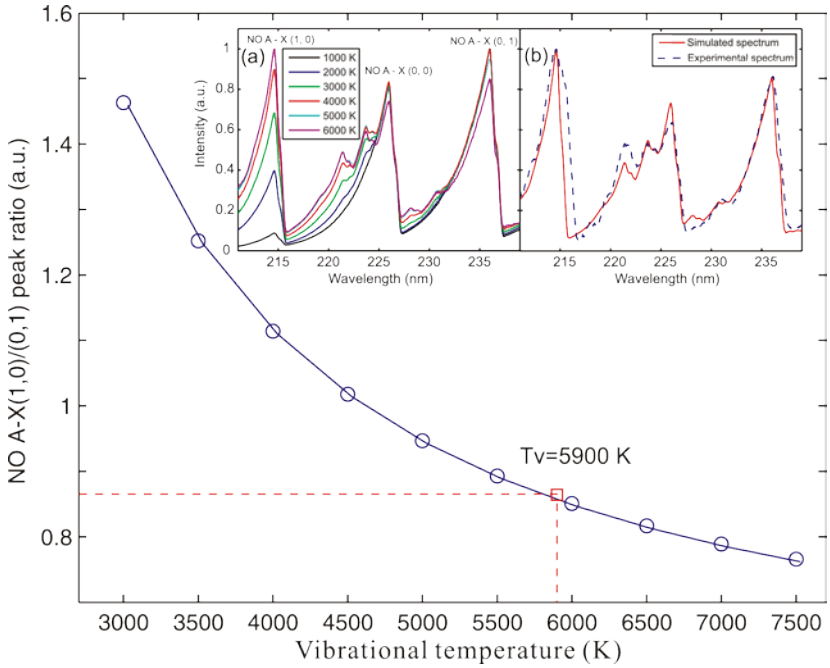

Fig. 5. Dependence of the vibrational temperature on the ratio of the peak intensities of the NO A–X (1, 0) and (0, 1) bands. The circles show the ratios simulated at different rotational temperatures whereas the square represents the one obtained by experiments. A vibrational temperature of 5900 K can be determined by comparing the ratios obtained from experiments and simulations. Figure 5(a) shows the simulated emission spectra of NO A–X at different vibrational temperatures. Figure 5(b) shows the experimental NO A–X spectrum of the gliding arc discharge is shown as an insert, as well as the simulated spectrum that was modeled at 5900 K vibrational temperature.

4.3 Electron temperature

The electron temperature can be estimated from the translational temperature and the reduced electric field strength using BOLSIG + (version 03/2016). An average translational temperature within the region of the plasma column is used to calculate the reduced electric field strength. The average temperature is obtained by averaging the temperature values in the hottest circle region with a diameter equal to the width of the plasma column. As shown in Fig. 6, the cross-sectional profile of intensity distributions of the emission intensity of the plasma columns are fitted by Gaussian functions. The full width at half maximum (FWHM) of the fitted curve is used to represent the width of the plasma column. It is found that the FWHM values of the two plasma columns are 0.70 and 0.88 mm, respectively. The images indicating the temperature distribution of the two plasma columns are shown as inserts in Fig. 6, and the hottest regions with a diameter equal to the width of the plasma column are marked in these images by circles. The average translational temperature within the marked region is found to be 1100 and 1050 K, respectively.

Determination of the electron temperature by use of BOLSIG + also relies on the input parameter of reduced electric field strength *E/N*. As shown in Eq. (4), it is possible to calculate the reduced electric field strength from the translational temperature, the voltage and the length of the plasma column. Since temporal and spatial variations are observed in the dynamic evolution of the gliding arc discharge, these three parameters should be determined using simultaneous multi-parameter measurements (SMM) so as to accurately determine the reduced electric field strength, as shown in Fig. 3. The length of the plasma column can be calculated by analyzing the images of the plasma columns. The boundary

pixels of the plasma column that forms a closed region are obtained. The number of boundary pixels of this closed region is summed, and the number of pixels divided by a factor of two was used as an estimate of the length in pixels. A grid image with known scales was recorded by the same camera and the number of pixels was converted to the real length. It is found that the lengths of the two plasma columns are 12.4 and 15.3 *cm*, respectively. Since the translational temperature, the voltage and the length of the plasma column are simultaneously obtained, the reduced electric field strength can be calculated by use of Eq. (4). The reduced electric field strength for the two plasma columns is calculated to be 5.6 and 6.1 *Td*, resulting in an estimate of the electron temperature of 8900 and 9300 *K*, respectively.

In the work published by Gangoli et. al. [32], the reduced electric field strength of a low-current gliding arc discharge was estimated to be 5-25 Td. The reduced electric field strength measured in this work is within this range. It should be noted that the reduced electric field strength can be underestimated if the size of the core plasma column (the electron channel) is smaller than the width of the plasma column measured from the plasma emission. The core plasma column has a much higher temperature than the surrounding region around it, and thus an overestimation of the size of the plasma column could underestimate the translational temperature of the plasma column and its reduced electric field strength. Korolev and associates [31] found that the reduced electric field strength of a low-current gliding arc discharge was about 30 Td with a gas temperature of about 4100 K in the plasma column.

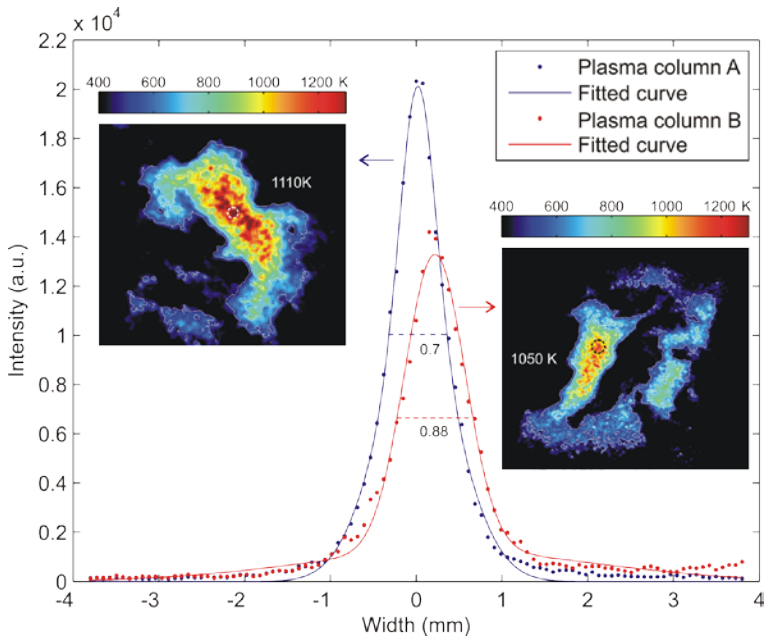

Fig. 6. Cross-sectional intensity distribution of the emission intensity of the plasma columns. The images of the two plasma columns are shown in Figs. 3 (a_4) and 3(b_4), respectively. The FWHM values (0.7 and 0.88 mm, respectively) of the fitted curves are used to represent the width of the plasma columns. The temperature distribution of the two plasma columns is inserted, and the hottest regions with a diameter equal to the width of the plasma column are marked in these images by circles. The average translational temperatures within the marked region are 1100 and 1050 K, respectively.

4.4 Uncertainty Analysis

The uncertainty of the translational temperature is mainly determined by some variables shown in Eq. (3), the Rayleigh signal of the air I_a, the Rayleigh signal of the gliding arc discharge I_g and the background signal I_b. The derivative of the translational temperature T_t with respect to these three variables can be obtained. The relative uncertainty of the

translational temperature T_t can be given by its derivative divided by the translational temperature T_t. The total uncertainty of the translational temperature δ_{Tt} is the root-sum-square value of all the three uncertainty sources and δ_{Tt} can be given by

$$\delta_{T_t} = \sqrt{(\theta_{I_a}\delta_{I_a})^2 + (\theta_{I_g}\delta_{I_g})^2 + (\theta_{I_b}\delta_{I_b})^2} \quad (5)$$

where θ and δ represent a sensitivity coefficient and a relative uncertainty of the corresponding signals mentioned above, respectively. According to Eq. (5), it can be estimated that the uncertainty of the translational temperature is approximately 24%.

The uncertainty of the electron temperature is mainly from the reduced electric field strength *E/N* since the electron temperature is dependent on the *E/N*. The total uncertainty of the reduced electric field strength $\delta_{E/N}$ can be calculated, yielding

$$\delta_{E/N} = \sqrt{(\theta_{T_t}\delta_{T_t})^2 + (\theta_L\delta_L)^2} \quad (6)$$

It should be noted that the term of the voltage in Eq. (4) is neglected in the uncertainty analysis since it can be accurately measured by the high-voltage probe. The uncertainty of the translational temperature δ_{Tt} was estimated to be 24% from above-mentioned calculations, whereas the length is, on average, underestimated by about 13% due to a 3D effect [45]. Thus, the uncertainty of reduced electric field strength

$\delta_{E/N}$ is approximately 27%. It can be obtained that the *E/N* of the gliding arc discharge is 5.6 ± 1.5 Td, which can be used to determine the uncertainty of the electron temperature through BOLSIG + . It is found that the electron temperature of the gliding arc discharge can be expressed as

$$7500K \le T_e \le 9900K \quad (7)$$

The uncertainty of the rotational and vibrational temperatures can be analyzed directly using SPECAIR. The method for determination of the rotational and vibrational temperatures is sensitive to the ratio of the two corresponding peaks. The rotational and vibrational temperatures of the gliding arc discharge measured in the experiments are estimated to be 4300 ± 400 K and 5900 ± 400 K, giving a relative uncertainty of 9% and 7%, respectively.

Table 1. Parameters of the gliding arc discharge and methods used for corresponding measurements.

Parameters	Gliding arc discharge	Methods
Translational temperature T_t	1100 ± 260 K	Rayleigh
Rotational temperature T_r	4300 ± 400 K	OES
Vibrational temperature T_v	5900 ± 400 K	OES
Reduced electric field strength *E/N*	5.6 ± 1.5 Td	SMM
Electron temperature T_e	8700 ± 1200 K	BOLSIG +

Parameters of the gliding arc discharge and methods used for the corresponding measurements are summarized in Table 1. The relatively large uncertainties of these temperatures are mainly due to the turbulence and unsteadiness of the gliding arc discharge. The gliding arc discharge takes a different form in every image even though the operating parameters and the timing are kept the same. In addition, other factors also contribute to the temperature uncertainties in the measurements. The uncertainty of the translational temperature is due to the shot-to-shot fluctuation of the laser energy, interference from Mie scattering and from other stray light. The use of filtered Rayleigh scattering [50] and structured illumination [52] is promising to reduce the uncertainty of the translational temperature. The dominant uncertainty sources of the rotational and vibrational temperature measurements are most likely the self-absorption, interference of overlapping emission lines and relatively insensitive dependence of the peak ratio on the temperature at a high temperature range. The uncertainty of the electron temperature primarily comes from the

indirect determination by use of the reduced electric field strength that is affected by the translational temperature and the length of the plasma column. Direct measurements of the electron temperature through Thomson scattering could possibly reduce the temperature uncertainty. However, the weak ionization and highly dynamic motion of the gliding arc discharge might lead to very low Thomson scattering signal levels.

5. Conclusions

Temperature measurements of a 35 kHz AC gliding arc discharge operated in a glow-type regime in atmospheric pressure air, including translational, rotational, vibrational and electron temperatures, were carried out using non-intrusive and in situ optical diagnostics.

The two-dimensional distribution of the translational temperature was measured by planar laser-induced Rayleigh scattering, indicating that the size of the hot region is about 4 – 11 times greater than the width of the plasma column. The peak translational temperature is about 1200 – 1500 *K* whereas the average translational temperature of the hottest region with a diameter equal to the width of the plasma column is about 1100 ± 260 *K*. The rotational and vibrational temperatures were determined by simulating the experimental spectra using the SPECAIR. The peak ratio of the P and R branches of the OH A–X (0, 0) band was used to determine the rotational temperature (4300 ± 400 K) of the gliding arc discharge, whereas the ratio of the peak intensities of the NO A–X (1, 0) and (0, 1) bands was employed to determine its vibrational temperature (5900 ± 400 *K*). The electron temperature (8700 ± 1200 K) was obtained using the BOLSIG + with simultaneously measured input parameters, including the translational temperature and the electric field strength.

The relations of these four different temperatures ($T_e > T_v > T_r > T_t$) suggest a high-degree non-equilibrium state of the gliding arc discharge operated in a glow-type regime. Especially, the rotational temperature of the gliding arc discharge used in our experiments is significantly larger than its translational temperature, showing that the translational and rotational degrees of freedom are far from equilibrium in this gliding arc discharge.

Funding

Swedish Energy Agency; the Swedish Research Council; the Knut & Alice Wallenberg Foundation; the European Research Council; and the National Natural Science Foundation of China (No. 51606217).